Journal of Chromatography, 548 (1991) 147–163
Elsevier Science Publishers B.V., Amsterdam

CHROMSYMP. 2255

High-performance liquid chromatography of amino acids, peptides and proteins

CXIII.[a] Predicting the performance of non-porous particles in affinity chromatography of proteins

Q. M. MAO, A. JOHNSTON, I. G. PRINCE and M. T. W. HEARN*
Department of Biochemistry and Centre for Bioprocess Technology, Monash University, Clayton, Victoria, 3168 (Australia)

ABSTRACT

A mathematical model, based on the Langmuir adsorption isotherm, has been developed to predict the performance of bioaffinity chromatography columns, packed with non-porous particles, in protein purification at the laboratory and preparative scales. Both the surface kinetics and the external film resistance as the rate controlling steps have been taken into account. The effects of particle size, fluid flow-rate and adsorbate concentration are examined. The model has been used to determine the forward interaction rate constant (k_1) for different adsorbate–ligand systems. Examples of the comparison between predicted and experimental breakthrough curves of a lysozyme–Cibacron Blue F3GA biomimetic affinity system are given. The influence of ionic strength and ligand density have also been evaluated.

INTRODUCTION

In recent years, non-porous monodisperse silica beads used as matrix supports in biochromatography (*e.g.* in biomimetic, hydrophobic and biospecific adsorption modes) have gained interest [1]. The main practical advantage of the non-porous packings in analytical and laboratory scale biochromatography with zonal elution systems is fast separation with high efficiency due to the absence of restrictive pore diffusion process with the adsorbates. Theoretical analyses on the behaviour of non-porous particles in biospecific adsorption processes, on the other hand, are largely lacking.

The literature on packed-bed adsorption theories and their applications to affinity chromatography has been reviewed extensively, see for example by Yang and Tsao [2] and Liapis [3]. In the concluding remarks of their review, Yang and Tsao pointed out that the lack of theoretical analysis on affinity chromatography was partly due to the difficulties encountered in solving the rigorous mathematical models.

[a] For part CXII, see ref. 20

0021-9673/91/$03.50

Certain simplifications must be made in order to obtain solutions. However, as most affinity chromatography systems display non-linear adsorption isotherm characteristics, the most important simplification of assuming a linear adsorption isotherm, which is often used as the basis of adsorption models, may be inappropriate. The models developed for affinity chromatography found in the literature [4–8] typically fall into two groups. In the first group a single mechanism is assumed to be the rate limiting step, either pore diffusion [5] or surface interaction [4], from which analytical solutions can be obtained. In the second group, the models are more rigorous as all of the possibly important rate limiting steps are considered [6–9]. Various numerical methods have been employed to solve these latter equations which concurrently result in excessive computation time.

The most important rate limiting steps in the biospecific adsorption processes have been identified as: external liquid film mass transfer; internal pore diffusion; and surface interaction [3,6]. For porous particles, pore diffusion resistance has been often considered as the rate controlling step [2,5]. There is no model explicitly developed for non-porous particles for which only the external film mass transfer resistance and the surface interaction rate are the rate limiting steps. The shortcoming of the non-porous particles is their limited surface area. Hence very small particles are preferred [1], subject to the pressure drop permitted in the system. Evidence exists that both the film mass transfer and the surface interaction can be important in determining the overall adsorption rate in systems with small particles [2,3,5].

Group two models attempt to interpret the physical basis of the mass transfer phenomenon by theoretical analysis, but the numerical procedures require special software packages [8] which are not always available. On the other hand, group one models have been found simple to use in preliminary evaluation of the column performance, but fail to address important parameters such as particle size and external film mass transfer coefficients. Hence a model, preferably capable of an analytical solution, yet which addresses both the external mass transfer and surface interaction would be desirable.

The central purpose of this work is to describe the development and method of analytical solution of a methematical model for non-porous particle systems which satisfies the above criteria. The straightforward nature of the resulting software allows utilization of the model on readily accessible equipment. The applicability of the model is demonstrated with a set of small scale experimental data generated in our laboratory, but the scope of the model and its intended application are directed towards predicting behaviour in preparative systems. Studies to confirm the suitability of the model in large scale equipment are currently underway.

THEORY

Non-porous particle adsorption model (NPPAM)

The non-porous particle adsorption model (NPPAM) has been developed to describe biospecific adsorption behaviour of non-porous particles in a packed bed. The basic assumptions of NPPAM are summarised as follows: (a) The effect of axial diffusion is negligible [3,9], and the fluid velocity is uniform over the cross-section of the column (eqn. 1). (b) The transport of adsorbate from the bulk fluid to the surface of the particle can be described by a film resistance mechanism (eqn. 2). (c) The

interaction between the adsorbate and the immobilized ligand at the particle surface is described by a Langmuir type model (eqn. 3). (d) The mass transfer and surface interaction steps are considered to occur in series (eqn. 4).

The continuity equation linking concentration, axial distance and time takes essentially the same form as those presented in the literature [10–12]:

$$\frac{U}{\varepsilon}\frac{\partial C}{\partial x} + \frac{\partial C}{\partial t} + \frac{1-\varepsilon}{\varepsilon}\frac{\partial q}{\partial t} = 0 \tag{1}$$

where U is the superficial liquid velocity, ε is the interstitial void fraction of the packed bed, x is the axial distance, t is time, C is the adsorbate concentration in the bulk of the liquid phase, and q is the adsorbate concentration in the solid phase.

The rate of mass transfer in the liquid film at the particle surface is described by

$$\frac{\partial C^*}{\partial t} = \frac{3}{R_0}\frac{1-\varepsilon}{\varepsilon}K_f(C - C^*) \tag{2}$$

where R_0 is the radius of the particle, K_f is the liquid film mass transfer coefficient, and C^* is the intermediate concentration of the adsorbate in the liquid phase at the surface of the particles. The term $(3/R_0)(1-\varepsilon)/\varepsilon$ is the interface area per unit interstitial void volume of the packed bed.

The surface interaction rate is described by the second-order reversible equation

$$\frac{\partial q}{\partial t} = k_1[(q_m - q)C^* - K_d q] \tag{3}$$

where k_1 is the forward interaction rate constant, q_m is the maximum adsorption capacity of the immobilized ligand, and K_d is the adsorption equilibrium constant.

As the film mass transfer and the surface interaction steps are considered to occur in series, the mass balance between the liquid concentration at the particle surface and the solid concentration can be written.

$$\varepsilon\frac{\partial C^*}{\partial t} = (1-\varepsilon)\frac{\partial q}{\partial t} \tag{4}$$

Eliminating C^* and its derivative from eqns. 2, 3 and 4 we get

$$\frac{\partial q}{\partial t} = \frac{Ak_1[(q_m - q)C - K_d q]}{A + k_1(q_m - q)} \tag{5}$$

where $A = \frac{3}{R_0}K_f$

Eqns. 1 and 5 are the basic equations of NPPAM in which both the film mass transfer and surface interaction rates are considered finite. Simplified cases may be derived from these two equations. In eqn. 5, if $K_f \to \infty$ then the surface interaction

(second-order kinetics) is considered as the rate controlling step. As a result, $A \gg k_1 (q_m - q)$ and the denominator on the right-hand side of eqn. 5 then can be put equal to A. Hence, when $K_f \to \infty$ eqn. 5 becomes

$$\frac{\partial q}{\partial t} = k_1[(q_m - q)C - K_d q] \tag{6}$$

On the other hand, if $k_1 \to \infty$ then the external mass transfer becomes the rate controlling step. As a result, $A \ll k_1 (q_m - q)$ and the denominator on the right-hand side of eqn. 5 can be put equal to $k_1 (q_m - q)$. Hence when $k_1 \to \infty$ eqn. 5 becomes

$$\frac{\partial q}{\partial t} = A\left(C - \frac{K_d q}{q_m - q}\right) \tag{7}$$

The solutions of these two simplified cases where a single mechanism was the rate limiting step have already been reported in the literature. The case of second-order kinetics controlling adsorption (eqn. 6) has been solved by Thomas [13]. The solution with external film resistance controlling adsorption (eqn. 7) has been presented by Hiester and Vermeulen [14].

The Thomas solution

The Thomas solution on fixed bed performance was originally developed for application to ion-exchange columns [13]. It has been shown [11,14] that the Thomas solution can be applied to the adsorption processes in general where the equilibrium relationship can be expressed by the Langmuir isotherm. At equilibrium, $q = q^*$, the attainable adsorption capacity of the adsorbent, and $C = C_0$, whilst $\partial q/\partial t$ in eqn. 6 can be put equal to zero since q is now constant. When such conditions apply, then the relationship between q^* and C_0 takes the familiar form

$$q^* = \frac{q_m C_0}{K_d + C_0} \tag{8}$$

By introducing the dimensionless terms:

$$X = \frac{C}{C_0}, \qquad Y = \frac{q}{q^*},$$

and

$$r^* = \frac{K_d}{K_d + C_0} \tag{9}$$

eqn. 6 can be rewritten as

$$\frac{\partial Y}{\partial t} = A_a[X(1 - Y) - r^* Y(1 - X)] \tag{10}$$

where

$$\Delta_a = k_1(K_d + C_0) = -\frac{k_1 C_0}{r^* - 1} \tag{11}$$

By defining the dimensionless time parameter τ and dimensionless distance parameter ζ such that

$$\zeta = \frac{x(1-\varepsilon)q^*\Delta_a}{UC_0} \tag{12}$$

$$\tau = \Delta_a\left(t - \frac{x\varepsilon}{U}\right) \tag{13}$$

the continuity eqn. 1 simplifies to

$$\frac{\partial X}{\partial \zeta} + \frac{\partial Y}{\partial \tau} = 0 \tag{14}$$

and eqn. 10 becomes

$$\frac{\partial Y}{\partial \tau} = [X(1 - Y) - r^* Y(1 - X)] \tag{15}$$

By appropriate substitution $\partial X/\partial\zeta$ can then be written as

$$\frac{\partial X}{\partial \zeta} = -[X(1 - Y) + r^* Y(1 - X)] \tag{16}$$

Assuming the bed is initially free of adsorbate, the boundary conditions are given by

$X = 1$ at $\zeta = 0$ for all τ
$Y = 0$ at $\tau = 0$ for all ζ

Thomas solved eqns. 15 and 16 and obtained a solution for the breakthrough curve which can be expressed in the following form [10,12,14]

$$\frac{C}{C_0} = \frac{\mathrm{J}(r^*\zeta,\tau)}{\mathrm{J}(r^*\zeta,\tau) + [1 - \mathrm{J}(\zeta,r^*\tau)]\exp[(r^* - 1)(\tau - \zeta)]} \tag{17}$$

The Hiester and Vermeulen approach

Hiester and Vermeulen [14] adapted the Thomas solution to solve the case where external film resistance is the rate controlling step. Introducing the dimensionless terms defined in the Thomas solution, eqn. 7 became

$$\frac{\partial Y}{\partial t} = \Delta_E[X(1 - Y) - r^* Y(1 - X)] \tag{18}$$

where

$$\Delta_E = \frac{AC_0}{q^*[1 + Y^*(r^* - 1)]} \tag{19}$$

Y^* was defined as an average value of q/q^*. As was suggested by Hiester and Vermeulen [14], Y^* has been given the numerical value $Y^* = 0.5$.

Here the time and distance parameters are defined as

$$\zeta = \frac{x(1 - \varepsilon)q^*\Delta_E}{UC_0} \tag{20}$$

$$\tau = \Delta_E\left(t - \frac{x\varepsilon}{U}\right) \tag{21}$$

so that eqn. 18 takes the form of eqn. 15 and the continuity eqn. 1 takes the form of eqn. 14. The boundary conditions remained unchanged. Therefore the solution given by eqn. 17 is applicable for the case where film resistance is controlling.

The solution for NPPAM

A similar method to that outlined above was adopted to obtain the solutions of the present model.

Introducing dimensionless terms, eqn. 5 becomes:

$$\frac{\partial Y}{\partial t} = \Delta_{aE}[X(1 - Y) - r^*Y(1 - X)] \tag{22}$$

where

$$\Delta_{aE} = \frac{AC_0}{q^*[1 + Y^*(r^* - 1)] - (A/k_1)(r^* - 1)} \tag{23}$$

The time and distance parameters are

$$\zeta = \frac{x(1 - \varepsilon)q^*\Delta_{aE}}{UC_0} \tag{24}$$

$$\tau = \Delta_{aE}\left(t - \frac{x\varepsilon}{U}\right) \tag{25}$$

Therefore eqns. 1 and 22 can be written in exactly the same dimensionless form as in the Thomas solution, *i.e.* eqns. 14, 15 and 16. The boundary conditions are still the same as in the Thomas solution. Hence the breakthrough curves can be calculated with eqns. 8, 9, 23–25, and 17.

It can be noted that the only difference in the three cases discussed is in the expressions of the terms Δ_a, Δ_E and Δ_{aE}, and

$$\frac{1}{\Delta_{aE}} = \frac{q^*[1 + Y^*(r^* - 1)]}{AC_0} - \frac{r^* - 1}{k_1 C_0} = \frac{1}{\Delta_E} + \frac{1}{\Delta_a} \tag{26}$$

Eqn. 26 is similar in form to that describing the total resistance of an electrical circuit with single resistances acting in series. This equation, therefore suggests that the rate limiting steps are also occurring in series.

The solution given by eqn. 17 contains the J function which is a complex function used in the solutions of many heat and mass transfer problems [10,14,16]. Numerical values of J function have been tabulated [10,15] and methods for calculating its value are also available [10,12,14,16]. A detailed procedure for evaluating the values of the J function is given in the Appendix. In these investigations, the NPPAM approach has been applied only to frontal chromatographic data. The application of NPPAM to a finite bath will be discussed in a separate paper.

EXPERIMENTAL

Packed bed adsorption data of a lysozyme–Cibacron Blue F3GA affinity system with non-porous particles was used in this work for evaluating the model predictions. The non-porous silica with a particle size of 1.5 μm was made as described in our previous publications [1,17,18] and is commercially available from Merck (Darmstadt, Germany). The non-porous silica was chemically modified with 3-mercaptopropyltrimethoxysilane (MPS) as described in ref. 17. The immobilization of Cibacron Blue F3GA on MPS-activated silica was performed as described in ref. 1. The dye affinity sorbent was packed into columns (19 × 4 mm I.D.). The mobile phase used was 0.1 *M* phosphate buffer with 1 *M* sodium chloride except for some cases where phosphate buffer only was used. The flow-rate was 0.5 ml/min. Details on materials, methods, equipment setup and operating procedures have been published previously [17,18].

RESULTS AND DISCUSSION

The NPPAM has been programmed in FORTRAN for easy transfer between PC and mainframe computers. As the computer code is short and simple, it is readily convertible to the different programming languages. Simulations of the adsorption process of proteins in fixed bed packed with non-porous particles have been carried out on an IBM PC/AT compatible machine. The effect of varying the rate constant, particle size, flow-rate and inlet concentration of protein in the liquid on the breakthrough curves are presented in Figs. 1–8. The dimensionless outlet concentrations were plotted against both the time and the amount of adsorbate applied to the column in cases with varying flow-rate and inlet concentration. The effect of varying both the adsorption equilibrium constant and the rate constant on the shape of the breakthrough curves are shown in Figs. 5–8. The maximum adsorption capacity of the particles (q_m) used in the model simulation was 1.6 mg/ml solid. The liquid film mass transfer coefficient (K_f) used was $3.5 \cdot 10^{-4}$ m/s except in Fig. 2 where K_f was estimated for different particle sizes using correlations discussed previously [9]. Other parameters

TABLE I

PARAMETERS USED IN MODEL SIMULATION

q_m = 1.6 mg/ml solid.

Fig. No.	d_p (μm)	C_0 (mg/ml)	Flow (ml/min)	k_1 (ml/mg s)	K_d (mg/ml)
1	1.5	0.1	0.5	0.25–1.0	0.08
2	1.5–200	0.1	0.5	2.0	0.08
3, 4	1.5	0.1	0.25–1.0	0.4	0.08
5, 6	1.5	0.1–0.4	0.5	0.4	0.08
7, 8	1.5	0.1–0.4	0.5	2.0	0.008

used are listed in Table I. Because the data available for the model evaluation was from laboratory scale columns, the parameters used in the model simulations largely correspond to these experimental conditions. However, there is no restriction for the NPPAM to be applied in the parameter range appropriate to the preparative scale.

For a saturated column, the amount of the adsorbate retained in the column, which is equal to the area behind the breakthrough curve [5,12] corresponds to the attainable adsorption capacity of the adsorbent q^*, as given in eqn. 8. In preparative affinity chromatography, however, the actual process would be terminated when the level of adsorbate in the effluent rises above a certain level, normally at less than 50% of the feed concentration [4,5,8]. In this case, a system with a sharp breakthrough curve would be much more efficient in utilising the column capacity than a system with a shallow one, as the amount of adsorbate retained when the process was terminated at the set concentration of the effluent, say *e.g.* 10% of that in the feed, is larger in the case with a sharper curve. Therefore, the breakthrough curves generated from the model simulation can be used to extract the performance information needed to optimize the process, such as the percentage utilisation of the column capacity, the amount of adsorbate lost in the effluent, and the processing time, etc. under various operating conditions. When comparing the sharpness of the breakthrough curves generated from different parameters, the appropriate variable for the abscissa corresponding to the parameter examined should be used, so that the area behind each curve is proportional to the amount adsorbed for every curve in the same graph. Hence, in evaluating the

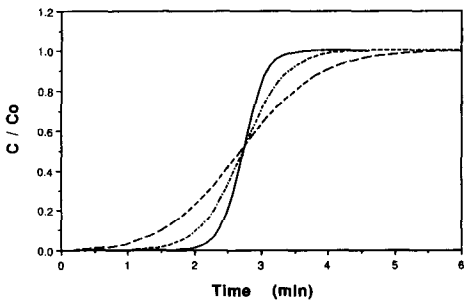

Fig. 1. Breakthrough curves simulated by NPPAM on the effect of forward interaction rate constant. [k_1 = 0.25 (– – –), 0.5 (– · – · –), 1.0 (———) ml/mg s].

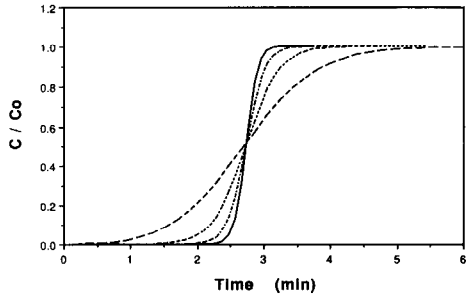

Fig. 2. Breakthrough curves simulated by NPPAM on the effect of particle diameter. ——— = 1.5; —·—·— = 50; ----- = 100 and — — — = 200 μm.

effect of flow-rate, the abscissa should be either the volume of the solution or the amount of the adsorbate applied, and in evaluating the effect of feed concentration the abscissa should be the amount of adsorbate applied.

Fig. 1 shows that a higher value of the surface interaction rate constant will lead to a sharper breakthrough curve and hence a more efficient system. However, the rate constant may not be adjustable as it is largely determined by the chosen protein–ligand system. In that case, the efficiency of the system can be improved by employing smaller particles as shown in Fig. 2. The sharper breakthrough curve of smaller particles is due to the increased mass transfer rate which is caused not only by the increased particle surface area, but also by the larger film mass transfer coefficient ($3.4 \cdot 10^{-4}$ for 1.5-μm particle compared with $1.2 \cdot 10^{-5}$ for 200-μm particle) as predicted from the literature correlation [9]. Fig. 3 shows the effect of flow-rate on processing time. As expected the lower flow-rate requires longer processing time. However, when the same curves were plotted against the amount of the adsorbate applied to the column, as shown in Fig. 4 it can be seen that lower flow-rate gives a sharper breakthrough curve. Hence, depending on the operating requirement (*e.g.* effluent concentration), an optimum flow-rate can be worked out from these model simulations which will not give the highest but the optimum percentage utilization of the column capacity that results in the highest processing rate.

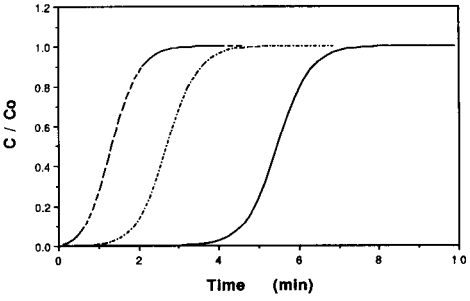

Fig. 3. Breakthrough curves simulated by NPPAM on the effect of flow-rate (——— = 0.25, —·—·— = 0.5, — — — = 1.0 ml/min) as a function of time.

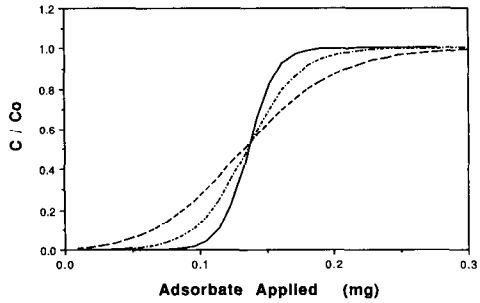

Fig. 4. Breakthrough curves simulated by NPPAM on the effect of flow-rate (——— = 0.25, —·—·— = 0.5, — — — = 1.0 ml/min), as a function of the amount of adsorbate applied.

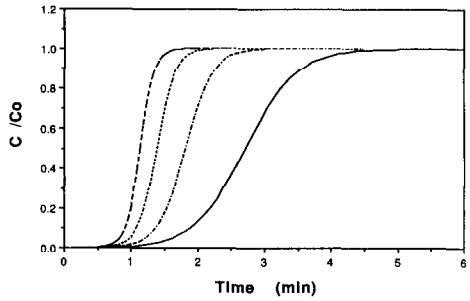

Fig. 5. Breakthrough curves simulated by NPPAM on the effect of inlet concentration, as a function of time for high value of K_d (0.08 mg/ml) and low value of k_1 (0.4). ——— = 0.1 mg/ml; —·—·— = 0.2 mg/ml; — — — = 0.3 mg/ml and — — — = 0.4 mg/ml.

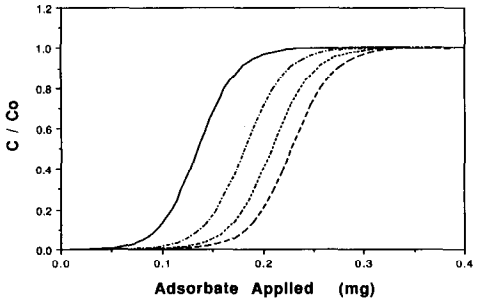

Fig. 6. Breakthrough curves simulated by NPPAM on the effect of inlet concentration, as a function of the amount of adsorbate applied for high value of K_d (0.08 mg/ml) and low value of k_1 (0.4). Denotation of lines as in Fig. 5.

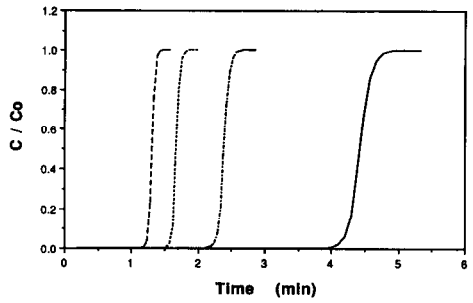

Fig. 7. Breakthrough curves simulated by NPPAM on the effect of inlet concentration, as a function of time for low value of K_d (0.008 mg/ml) and high value of k_1 (2.0). Denotation of lines as in Fig. 5.

The effect of varying the inlet concentration of the adsorbate on the predicted breakthrough curves is shown in Figs. 5 to 8. Figs. 5 and 7 show the effect on the processing time, and Figs. 6 and 8 show the effect on the column efficiency. From eqn. 8 it can be seen that the amount of adsorbate retained in the column is a function of both the feed concentration C_0 and the adsorption equilibrium constant K_d provided that the maximum adsorption capacity q_m is held constant. Increasing C_0 will increase the amount of protein adsorbed and cause the breakthrough curves to shift to the right as is the case in Figs. 6 and 8. The sharpness of the curves, on the other hand, was not influenced by the change in C_0. The improved column efficiency at higher C_0 is mainly due to the increased amount of the adsorbate retained. As listed in Table I, higher value of k_1 and lower value of K_d were used to generate the breakthrough curves presented in Figs. 7 and 8. More adsorbate was retained in the column for this system compared with the system illustrated in Figs. 5 and 6 at the same values of C_0. However, the change of the amount adsorbed on the column to the variation of C_0 in Fig. 8 is not as sensitive as for the system shown in Fig. 6.

From the model simulations shown in Figs. 1 to 8 it can be seen that NPPAM is a useful tool in evaluating the binding performance of affinity adsorption columns with non-porous particles. It takes only seconds to generate a breakthrough curve on

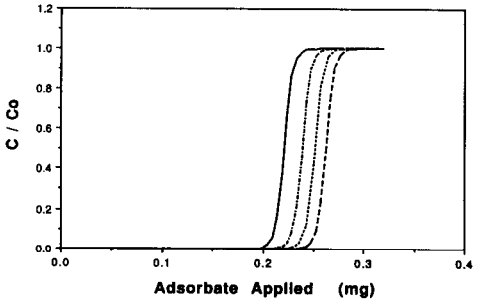

Fig. 8. Breakthrough curves simulated by NPPAM on the effect of inlet concentration, as a function of the amount of adsorbate applied for low value of K_d (0.008 mg/ml) and high value of k_1 (2.0). Denotation of lines as in Fig. 5.

a normal PC, which is particularly useful in fitting experimental curves where hundreds of iterations may be necessary. As discussed above, the amount of the adsorbate retained in the column is equal to the area behind the breakthrough curve. Therefore, numerical integration of the breakthrough curves generated from the model simulation may serve as a check of the accuracy of the model prediction. Calculation shows that the difference between the amount adsorbed calculated from eqn. 8 and the integrated result is always less than 0.01%.

One point requiring discussion on the NPPAM is that in its solution there is an approximation of Y^*, inherited from the Hiester and Vermeulen's method [12,14]. Although $Y^* = q/q^*$ is a variable since q varies with time, it was necessary to assign to Y^* a constant value in order to use the Thomas solution. $Y^* = 0.5$ was used in the model simulation throughout this paper, as suggested by Hiester and Vermeulen [14]. Therefore, the effect of the value of Y^* on the shape of the breakthrough curves and the area behind the curves predicted by the model should be closely monitored. Calculations were carried out using $Y^* = 0.1$, 0.5 and 0.9. It was found that the value of Y^* has no influence on the area behind the breakthrough curves. For most conditions used in the present model simulation, the effect of varying Y^* on the shape of the breakthrough curve is also negligible in the range of $Y^* = 0.1$ to 0.9. In some extreme cases, the curve with $Y^* = 0.9$ is slightly sharper than the one with $Y^* = 0.1$. The method to calculate breakthrough curves in cases where the effect of the Y^* value can not be neglected has been discussed by Hiester and Vermeulen [14].

Beside predicting the performance of a packed bed for given operating conditions and system parameters, the model can also be used for fitting parameters to packed bed experimental results to derive system kinetic data such as the surface interaction rate constant and the mass transfer coefficient, as well as to verify thermodynamic data. Figs. 9–12 show the comparison between the predicted and the experimental breakthrough curves for lysozyme adsorption to a biomimetic dye affinity sorbent. In Figs. 9–12 the points are the experimental data and the lines are the model predictions. The ligand used was Cibacron Blue F3GA and the mobile phase used was 0.1 *M* phosphate buffer with 1 *M* sodium chloride except for the case in Fig. 12 where phosphate buffer only was used. The reason for using sodium chloride in the

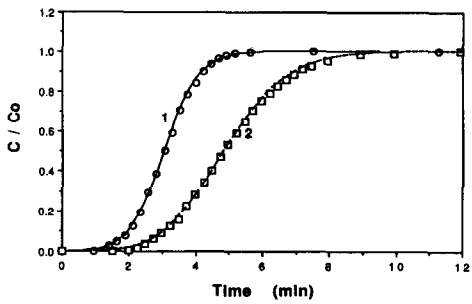

Fig. 9. Predicted (lines) and experimental (points) breakthrough curves for the adsorption of lysozyme on Cibacron Blue F3GA immobilized on 1.5 μm diameter non-porous silica particles. Mobile phase: 0.1 *M* phosphate buffer with 1 *M* sodium chloride. Flow-rate = 0.5 ml/min. Column: 19 mm long and 4 mm I.D. K_d = 0.073 mg/ml, C_0 = 0.013 (□) and 0.075 (○) mg/ml. For other parameters related to predicted curves (1 and 2) see Table II.

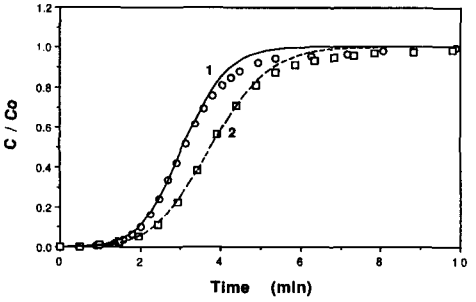

Fig. 10. Predicted (lines) and experimental (points) breakthrough curves for lysozyme adsorption. Mobile phase: 0.1 *M* phosphate buffer with 1 *M* sodium chloride. K_d = 0.073 mg/ml, C_0 = 0.036 (□) and 0.057 (○) mg/ml. For other experimental parameters see legend of Fig. 9.

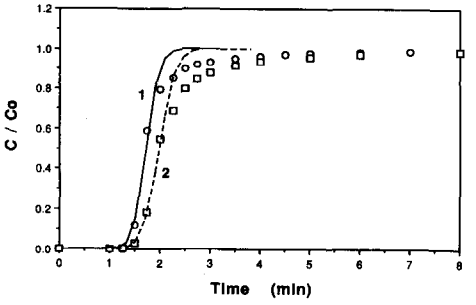

Fig. 11. Predicted (lines) and experimental (points) breakthrough curves for lysozyme adsorption. Mobile phase: 0.1 *M* phosphate buffer with 1 *M* sodium chloride. K_d = 0.23 mg/ml, C_0 = 0.04 (□) and 0.1 (○) mg/ml. For other experimental parameters see legend of Fig. 9.

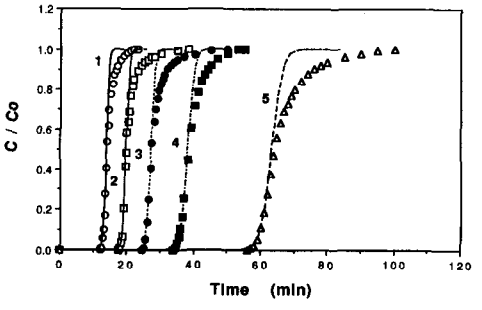

Fig. 12. Predicted (lines) and experimental (points) breakthrough curves for lysozyme adsorption with high ligand density. Mobile phase: 0.1 *M* phosphate buffer. C_o = 0.100 (○); 0.065 (□); 0.045 (●); 0.030 (■) and 0.018 (△) mg/ml. For other experimental parameters see legend of Fig. 9 and Table II. For other parameters related to predicted curves (1–5) see Table II.

TABLE II

RESULTS OF MODEL PREDICTION

Fig. No.	Curve No.	C_0 (mg/ml)	q_m (mg/ml solid)	K_d (mg/ml)	k_1 (ml/mg s)
9	1	0.075	1.503	0.073	0.375
	2	0.013	1.430		0.596
10	1	0.057	1.326	0.073	0.456
	2	0.036	1.385		0.467
11	1	0.100	1.781	0.230	1.218
	2	0.040	1.700		1.753
12	1	0.100	5.030	0.0055	0.448
	2	0.065	4.825		0.565
	3	0.045	4.722		0.648
	4	0.030	4.671		0.605
	5	0.018	5.082		0.648

mobile phase was to suppress non-specific binding phenomena. The film mass transfer coefficient was predicted from correlations in the literature [9] and a value of $3.4 \cdot 10^{-4}$ m/s was used. The maximum adsorption capacity q_m and the equilibrium constant K_d were derived from the experimental data.

A subroutine was written to find the appropriate value of the forward surface interaction rate constant k_1 which would give a satisfactory fit to the experimental curve. The objective function chosen to be minimized is the sum of the squares of the percentage deviation between predicted and experimental values of C/C_0, over the range of $C/C_0 = 0.01$ to 0.95 on the experimental breakthrough curve. This practice gave a much greater weight to the initial part of the curve in the minimization process. Therefore, in cases where a good fit to the whole breakthrough curve is not possible, the initial part of the curve would have a close fit, as in an actual process the adsorption phase would be terminated at less than 50% breakthrough [5]. In order to obtain the best fit, q_m has also been adjusted. The rate constant (k_1) obtained and the parameters used are listed in Table II.

The agreement between model prediction and experimental data is quite good in Fig. 9. However, the model could only fit the initial part of the experimental breakthrough curves well in most cases in Figs. 10, 11 and 12. In every case where deviation from the experimental data occurred, the model always predicted that the column approached saturation faster than that indicated by the experiment. This phenomenon has been reported in the literature for both porous [8] and non-porous [9] particles. In their adsorption study of lysozyme–anti-lysozyme system with non-porous silica particles, Liapis *et al.* [9] suggested that non-specific interaction between lysozyme and the silica may be responsible for the disagreement between model prediction and experimental data. Initially most of lysozyme molecules would interact with anti-lysozyme which was fast, hence specific adsorption was dominant. As time progressed, the dominant adsorption mechanism switched to non-specific adsorption which was slower, hence the overall adsorption rate decreased. This point was supported by the experimental data for a system with a higher ligand density which

showed better agreement between measured and predicted breakthrough curves. These workers proposed that the amount of non-specific surface area compared to the area of the particles covered by the ligand was lower in the system with the antibody immobilized to high (average) density. However, the trend was reversed in the present study where the system with higher ligand density showed poorer agreement between predicted and measured breakthrough curves, as shown in Table II and Figs. 9–12. In this case, heterogeneity in the ligand distribution and the resulting steric hindrance might be the main cause of the slow adsorption when the column approaches protein saturation.

CONCLUSIONS

It can be concluded that NPPAM in its present form has already shown promising features in predicting the performance of non-porous particles in affinity chromatography for both laboratory and preparative systems. As the model allows independent evaluation of the factors affecting the protein–ligand interaction, as well as the factors affecting the mass transfer behaviour of the proteins, the model is compatible to those more sophisticated models [7,8]. The simplicity of the model not only allows shorter running time, but also makes the modification and adaptation of the model easier. The model simulations have shown that for the affinity chromatography columns employing non-porous particles, column efficiency can be improved by using smaller particles, moderate flow-rate, and employing a protein–ligand system with reasonably fast interaction rates. The deviation of the experimental data from the model prediction may be due to the effect of heterogeneity in the ligand distribution and other mass transfer process, as well as different adsorption mechanisms.

APPENDIX

The J function

The solution of the models requires the knowledge of the J function which took the form of [10,12,14]

$$J(\alpha, \beta) = 1 - \int_0^{\alpha} e^{-(\alpha+\lambda)} I_0(2\sqrt{\beta\lambda}) d\lambda \tag{A1}$$

where I_0 is a modified Bessel function of the first kind. The numerical value of the J function lies between zero and one, and where $J(0,\beta) = 1.0$ and $J(\alpha,0) = e^{-\alpha}$.

When both α and β are large (>10), Thomas suggested the following approximation [14]

$$J(\alpha,\beta) = \frac{1}{2}\left[1 - \mathrm{erf}(\sqrt{\alpha} - \sqrt{\beta}) + \frac{e^{-(\sqrt{\alpha}-\sqrt{\beta})^2}}{\sqrt{\pi}(\sqrt{\beta} + \sqrt[4]{\alpha\beta})}\right] \tag{A2}$$

According to Hiester and Vermeulen [14], eqn. A2 is accurate to within 1% when $\alpha\beta \geqslant 36$. The error function in the equation can be calculated from [19]

$$\mathrm{erf}(x) = \frac{2}{\sqrt{\pi}}\left[x + \sum_{k=1}^{n}(-1)^k \frac{x^{(2k+1)}}{k!(2k+1)}\right] \tag{A3}$$

It was found when $n \geqslant 30$, the difference between calculated value and the tabulated value of the error function in the literature [12,19] is less than 0.0001.

For smaller value of α and β, a formula used by Tan [16] gives a better approximation.

$$J(\alpha,\beta) = 1 - e^{-\beta}\sum_{k=0}^{n}\frac{\beta^k A_k(\alpha)}{k!k!} \tag{A4}$$

where

$$A_0(\alpha) = 1 - e^{-\alpha}$$

$$A_k(\alpha) = kA_{k-1}(\alpha) - \frac{\alpha^k}{e^{\alpha}} \qquad \text{for } k \geqslant 1$$

Calculation has shown that for $(\alpha + \beta) \leqslant 75$ and $\alpha \leqslant 35$, the difference between the result of eqn. A4 and the tabulated value of the J function [10,15] is less than 0.00002. For $(\alpha + \beta) > 75$ or $\alpha > 35$, eqn. A2 is accurate to within 0.0001 compared with tabulated data.

SYMBOLS

C Liquid phase concentration.
C_0 Inlet liquid concentration.
C^* Intermediate liquid concentration.
k_1 Forward interaction rate constant.
K_d Adsorption equilibrium constant.
K_f Liquid film mass transfer coefficient.
q Solid phase concentration.
q_m Maximum solid adsorption capacity.
q^* Attainable adsorption capacity of the adsorbent (eqn. 8).
R_0 Particle radius.
r^* Equilibrium parameter (eqn. 9).
t Time.
U Superficial liquid velocity.
X $= C/C_0$.
Y $= q/q^*$.
x Axial distance.

ε Adsorption column void fraction.
τ Dimensionless time parameter.
ζ Dimensionless distance parameter.

ACKNOWLEDGEMENT

This project was supported by a grant provided by the Australian Research Council. The assistance provided by Mr. H.-J. Wirth in obtaining experimental data is greatly appreciated.

REFERENCES

1 F. B. Anspach, K. K. Unger, J. Davies and M. T. W. Hearn, *J. Chromatogr.*, 457 (1988) 195.
2 C. Yang and G. T. Tsao, *Adv. Biochem. Eng.*, 25 (1982) 1.
3 A. I. Liapis, *J. Biotechnol.*, 11 (1989) 143.
4 H. A. Chase, *J. Chromatogr.*, 297 (1984) 179.
5 F. H. Arnold, H. W. Blanch and C. R. Wilke, *Chem. Eng. J.*, 30 (1985) B9.
6 B. H. Arve and A. I. Liapis, *AIChE J.*, 33 (1987) 179.
7 B. H. Arve and A. I. Liapis, *Biotechnol. Bioeng.*, 32 (1988) 616.
8 B. J. Horstmann and H. A. Chase, *Chem. Eng. Res. Des.*, 67 (1989) 243.
9 A. I. Liapis, B. Anspach, M. E. Findley, J. Davies, M. T. W. Hearn and K. K. Unger, *Biotechnol. Bioeng.*, 34 (1989) 467.
10 T. K. Sherwood, R. L. Pigford and C. R. Wilke, *Mass Transfer*, McGraw-Hill, New York, 1975.
11 J. M. Coulson and J. F. Richardson, *Chemical Engineering*, Vol. 3, Pergamon Press, Oxford, 2nd ed., 1979.
12 A. L. Hines and R. N. Maddox, *Mass Transfer, Fundamentals and Applications*, Prentice-Hall, Englewood Cliffs, NJ, 1985.
13 H. G. Thomas, *J. Am. Chem. Soc.*, 66 (1944) 1664.
14 N. K. Hiester and T. Vermeulen, *Chem. Eng. Prog.*, 48 (1952) 505.
15 F. Helfferich, *Ion Exchange*, McGraw-Hill, New York, 1962.
16 H. Tan, *Chem. Eng.*, Oct. 24 (1977) 158.
17 F. B. Anspach, A. Johnston, H.-J. Wirth, K. K. Unger and M. T. W. Hearn, *J. Chromatogr.*, 476 (1989) 205.
18 F. B. Anspach, A. Johnston, H.-J. Wirth, K. K. Unger and M. T. W. Hearn, *J. Chromatogr.*, 499 (1990) 103.
19 E. Kreyszig, *Advanced Engineering Mathematics*, John Wiley & Sons, New York, 6th ed., 1988.
20 A. Johnston, Q. M. Mao and M. T. W. Hearn, *J. Chromatogr.*, 548 (1991) 127.